

Heat engines and heat pumps in a hydrostatic atmosphere: How surface pressure and temperature constrain wind power output and circulation cell size

A. M. Makarieva^{1,2*}, V. G. Gorshkov^{1,2}, A.V. Nefiodov¹,
D. Sheil³, A. D. Nobre⁴, P. Shearman^{5,6}, B.-L. Li²

¹Theoretical Physics Division, Petersburg Nuclear Physics Institute, 188300 Gatchina, St. Petersburg, Russia, ²XIEG-UCR International Center for Arid Land Ecology, University of California, Riverside 92521-0124, USA, ³Norwegian University of Life Sciences, Ås, Norway, ⁴Centro de Ciência do Sistema Terrestre INPE, São José dos Campos SP 12227-010, Brazil ⁵UPNG Remote Sensing Centre, Biology Department, University of Papua New Guinea, Papua New Guinea, ⁶School of Botany and Zoology, The Australian National University, Canberra, Australia.

Abstract

The kinetic energy budget of the atmosphere's meridional circulation cells is analytically assessed. In the upper atmosphere kinetic energy generation grows with increasing surface temperature difference ΔT_s between the cold and warm ends of a circulation cell; in the lower atmosphere it declines. A requirement that kinetic energy generation is positive in the lower atmosphere limits the poleward cell extension L of Hadley cells via a relationship between ΔT_s and surface pressure difference Δp_s : an upper limit exists when Δp_s does not grow with increasing ΔT_s . This pattern is demonstrated here using monthly data from MERRA re-analysis. Kinetic energy generation along air streamlines in the boundary layer does not exceed 40 J mol^{-1} ; it declines with growing L and reaches zero for the largest observed L at 2 km height. The limited meridional cell size necessitates the appearance of heat pumps – circulation cells with negative work output where the low-level air moves towards colder areas. These cells consume the positive work output of the heat engines – cells where the low-level air moves towards the warmer areas – and can in theory drive the global efficiency of atmospheric circulation down to zero. Relative contributions of Δp_s and ΔT_s to kinetic energy generation are evaluated: ΔT_s dominates in the upper atmosphere, while Δp_s dominates in the lower. Analysis and empirical evidence indicate that the net kinetic power output on Earth is dominated by surface pressure gradients, with minor net kinetic energy generation in the upper atmosphere. The role of condensation in generating surface pressure gradients is discussed.

1 Introduction

The Earth has three meridional circulation cells in each hemisphere: Polar, Ferrel and Hadley. In the first and last the air moves from the cold to the warm areas in the lower atmosphere returning in the upper atmosphere, while in the intermediate cell the relationship between the air motion and temperature gradient is reversed. Why do we find this pattern of cells rather than say one cell in each hemisphere stretching from the equator to the pole? What determines the size of the existing cells? Besides their theoretical significance, these questions have practical implications (Webster, 2004). Shifting cell boundaries can lead to

*Corresponding author. E-mail: ammakarieva@gmail.com

marked climatic changes such as the decrease of rainfall observed in the subtropics (e.g., Bony et al., 2015; Heffernan, 2016).

On a rotating planet the maximum poleward extension of the meridional circulation cells in the upper atmosphere is related to conservation of angular momentum. As the air moves poleward and approaches the Earth's rotation axis, the air velocity must increase provided angular momentum is conserved. In the limit, at the pole, the air would need to reach an infinite velocity. The energy for this acceleration is derived from the pressure gradient in the upper troposphere, which is associated with meridional temperature gradient. At a given height in the upper troposphere, air pressure above the warm areas is higher than it is over cold areas. The greater the temperature gradient, the further it can push the air towards the pole. Thus, for a meridional flow conserving angular momentum the maximum cell size grows with increasing temperature difference between the equator and the pole.

If the angular momentum is not conserved but decreases as the air moves from the equator to the pole, the air velocity increases more slowly. Then, for the same temperature difference, the meridional cell can reach further towards the pole. The degree to which angular momentum is conserved is controlled by turbulent friction, which determines the exchange of angular momentum between different atmospheric layers and the Earth. Formally, in global circulation models turbulent friction is governed by several parameters like surface drag, eddy diffusivity and orography. The effect of turbulent friction on the extension of circulation cells has received considerable attention from different perspectives (Held and Hou, 1980; Robinson, 1997; Schneider, 2006; Chen et al., 2007; Marvel et al., 2013). For example, in the absence of orography if eddy diffusivity is exactly zero, the meridional cells do not exist. If, on the other hand, turbulent friction in the upper atmosphere is sufficiently large, then the meridional circulation cells can extend to the poles (see, e.g., Marvel et al., 2013, their Fig. 3).

Provided there is sufficient information on turbulent friction, the extension and intensity of the meridional circulation cells can be retrieved by solving the equations of motion. However, turbulent processes themselves depend on the nature and intensity of the large-scale circulation that they help to arrange. Furthermore, turbulent eddies on different scales can have their local energy sources rather than being simply products of dissipation of the large-scale motions. Since the general theory of atmospheric turbulence is absent, model parameters that govern turbulent friction in circulation models cannot be specified a priori. Instead, they are chosen such that the resulting circulation conforms to observations. However, given the crucial role of the general circulation for the planetary climate (see, e.g., Bates (2012) and Shepherd (2014) for two complementary perspectives), the fact that turbulent processes cannot be formulated from theory hampers reliable predictions of future climates.

In this situation it is relevant to search for physical constraints to which the atmosphere obeys which could govern formulation of the dissipative processes in the atmosphere. In this paper we consider the process of kinetic energy generation in the upper and lower atmosphere and how it can be expressed via the values of surface pressure and temperature.

Why is kinetic energy generation relevant and how does it relate to turbulence? In a stationary atmosphere the rate of kinetic energy generation is equal to the rate at which wind power dissipates via turbulent processes. However, unlike turbulence, kinetic energy generation can be easily formulated in terms of measurable atmospheric variables. Kinetic energy is generated by pressure gradients: wind power (the rate of kinetic energy generation) per unit air volume is equal to the scalar product of air velocity and pressure gradient (e.g., Boville and Bretherton, 2003). Consider for simplicity an axisymmetric atmosphere. If eddy diffusivity is zero, the air is in geostrophic equilibrium and rotates around the Earth along the isobars everywhere except at the surface where wind velocity is zero. Since in geostrophic balance air velocity is everywhere perpendicular to pressure gradient, the wind power is zero. No heat engines and no thermodynamic cycles exist on such an Earth. This means that turbulence not only controls the non-conservation of angular momentum

along the streamlines of a large-scale circulation. It also ultimately determines whether there is a heat engine operating on Earth and how much power it generates.

The concept of Carnot heat engine as applied to the atmosphere has been considered by many authors attempting to constrain the efficiency of atmospheric circulation (Wulf and Davis Jr., 1952; Peixoto and Oort, 1992; Lorenz and Rennó, 2002; Pauluis et al., 2000; Pauluis, 2011; Kieu, 2015). The heat source is the warm Earth's surface and the heat sink is associated with a higher altitude and/or latitude. Despite the prevalence of the Carnot cycle concept in the meteorological literature no established relationships show how work output depends on pressure and temperature differences at the Earth's surface. Here we develop such relationships for a Carnot cycle (Section 3) and for a more realistic cycle where the non-vertical streamlines go parallel to the surface at a constant height (Section 4). We show that kinetic energy generation along air streamlines in the lower atmosphere and in the upper atmosphere have opposite relationships on surface temperature difference. The greater the temperature difference between the warmer and the colder ends of the circulation in a heat engine, the more kinetic energy is generated in the upper atmosphere and less in the lower.

We then show that the condition that the kinetic energy generation must be positive in the lower atmosphere limits the horizontal dimension of the cell via a relationship between Δp_s and ΔT_s . An upper limit exists when Δp_s does not grow with increasing ΔT_s . Using data from MERRA re-analysis (Rienecker et al., 2011) we investigate the dependence between Δp_s and ΔT_s for Hadley cells to find that this pattern matches the observations (Section 5).

In Section 6 we use the developed expressions to evaluate the kinetic energy generation budget in the atmosphere composed of several heat engines (cycles with positive work output, Hadley and Polar cells) and heat pumps (cycles with negative work output, Ferrel cells). We show that our theoretical estimates are consistent with direct assessments of kinetic energy generation by the Earth's meridional circulation cells (Section 7). We then consider the high-resolution estimates of global rates of kinetic energy generation by Huang and McElroy (2015) and find that the net kinetic energy generation in the upper atmosphere is relatively small. We infer that on Earth the surface pressure gradients are the principle determinants of the global kinetic power budget.

2 Kinetic energy generation and total work output in a thermodynamic cycle

In a hydrostatic atmosphere kinetic energy is mostly generated by horizontal pressure gradients. On the other hand, major pressure differences are associated with the vertical dimension. We start our analysis by considering how kinetic energy generation relates to the total work A of a thermodynamic cycle.

We use the ideal gas law

$$pV = RT, \quad pdV = RdT - Vdp, \quad (1)$$

where $R = 8.3 \text{ J mol}^{-1} \text{ K}^{-1}$ is the universal gas constant, p is pressure, T is temperature and V ($\text{m}^3 \text{ mol}^{-1}$) is molar volume, and the condition of hydrostatic equilibrium

$$\rho \mathbf{g} = \nabla_z p, \quad (2)$$

where $\rho = M/V$ is air density, M is air molar mass and \mathbf{g} is the vector of gravity acceleration.

Using the definition of horizontal velocity $u_h \equiv dy/dt$ and vertical velocity $w \equiv dz/dt$ we find

$$A \equiv \oint pdV = - \oint V \frac{dp}{dt} dt = - \oint V \frac{\partial p}{\partial y} \Big|_{z=z(y)} dy, \quad (3)$$

as far as from (2) we have

$$-\oint V \frac{\partial p}{\partial z} \Big|_{y=y(z)} dz = \oint V \rho g dz = Mg \oint dz = 0. \quad (4)$$

Here $y = y(z)$ and $z = z(y)$ are the equations of the closed streamline that defines the cycle, where z is height and y is horizontal coordinate. Eq. (3) shows that for any thermodynamic cycle where the mass of gas is constant, total work A (J mol^{-1}) is equal to total kinetic energy generation – and this depends solely on horizontal pressure gradients. In an atmosphere where water vapor undergoes phase transitions, Eq. (3) still describes kinetic energy generation per mole circulating air with reasonable accuracy (see 8 for details).

We emphasize that the obtained expression (3) for kinetic energy generation do not carry any information about planet rotation and universally apply to any air streamlines, on rotating as well as on non-rotating planets. This is because the Coriolis force that distinguishes the equations of motions on a rotating planet from non-rotating one is by definition perpendicular to air velocity. In the result, it makes no contribution to wind power (kinetic energy generation per unit time). Thus, while wind *velocity* can be approximately retrieved from the assumption of geostrophic balance, wind *power* cannot. Wind power is non-zero to the degree by which the geostrophic balance is broken.

3 Kinetic energy generation and cell size limit in a Carnot cycle

We will now derive the dependence of kinetic energy generation on surface pressure and temperature differences in a Carnot cycle. A Carnot cycle derives work from a given temperature gradient (heat engine) or uses external work to generate a temperature gradient (a heat pump). In theory the Carnot cycle requires that these processes are reversible and thus performed with maximum efficiency. In the atmosphere this idealized cycle involves a heat flow from a warmer region (the heat source) to a colder region (the heat sink) in a heat engine or in reverse direction in a heat pump. A Carnot cycle consists of two isotherms and two adiabates (Fig. 1a). Work outputs on the two adiabates have different signs and sum to zero. Total work output $A \equiv \oint p dV$, where p is pressure and V is molar volume, is equal to the sum of work outputs on the two isotherms. It can be written as (for a derivation see, e.g., Makarieva et al., 2010)

$$A = -R(T^+ - T^-) \ln \left(1 + \frac{\Delta p_C}{p} \right) \approx -R(T^+ - T^-) \frac{\Delta p_C}{p}. \quad (5)$$

Here T^+ and $T^- < T^+$ are the temperatures of the two isotherms, p is the pressure that the air has as it starts moving along the warmer isotherm and Δp_C is the pressure change along the warmer isotherm, $|\Delta p_C| \ll p$. If the air expands at the warmer isotherm (cycle ABCDA), we have $\Delta p_C < 0$ and $A > 0$. The Carnot cycle is then a true heat engine: it does work on the external environment and transports heat from the heat source to the heat sink (Fig. 1a). If the air contracts at the warmer isotherm (cycle BADCB) we have $\Delta p_C > 0$ and $A < 0$. The Carnot cycle functions now as a heat pump: it transports heat from the heat sink (cold area) to the heat source (warm area) consuming work from the external environment.

We consider a closed streamline where the adiabates are vertical. If the atmosphere is horizontally isothermal, then the isothermal parts of the streamline lie parallel to the surface and the work output of the cycle is determined by surface pressure difference $\Delta p_C = -\Delta p_s$ (Fig. 1b). If there is a horizontal temperature gradient at the surface, then the isotherms are no longer horizontal, but have an inclination that depends on the magnitude of the

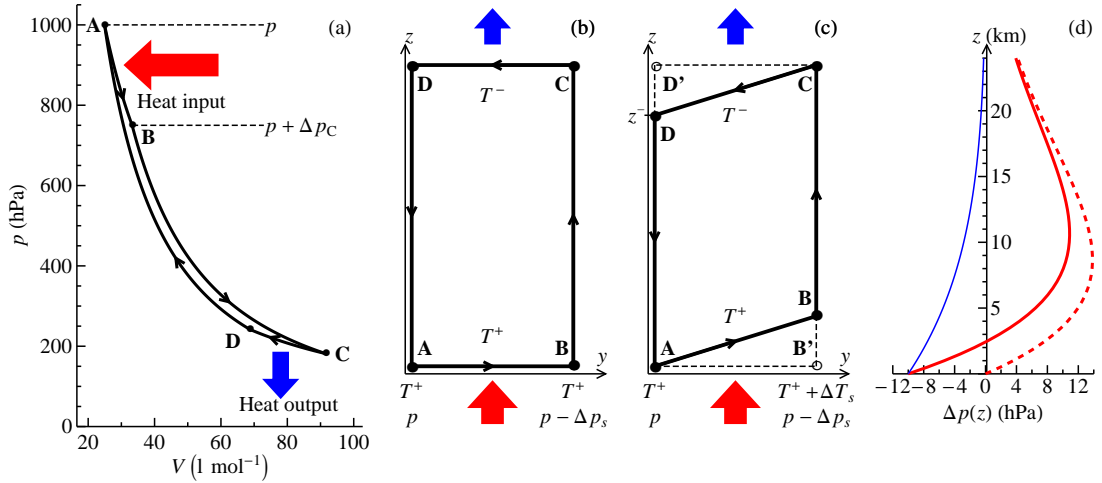


Figure 1: Hydrostatic Carnot heat engine. (a) Carnot cycle with typical atmospheric parameters: $p = 1000$ hPa, $T^+ = 300$ K (isotherm AB), $T^- = 200$ K (isotherm CD), $\Delta p_C = -250$ hPa. Work output at the warmer (colder) isotherm is equal to heat input (output). BC and DA are adiabats. (b,c) The same cycle in spatial coordinates y, z in (b) horizontally isothermal atmosphere ($\Delta T_s = 0$ K) and (c) in the presence of a horizontal temperature difference ($\Delta T_s > 0$ K). (d) Differences in pressure at height z for atmospheric columns above points A and B', where pressure and temperature follow Eqs. (6) and (7) with surface pressure and temperature equal to $p_A = 1010$ hPa, $T_A = 300$ K and $p_{B'} = p_A - \Delta p_s$, $T_{B'} = T_A + \Delta T_s$ at points A and B', respectively; solid blue line: $\Delta p_s = 10$ hPa, $\Delta T_s = 0$ K; dashed red line: $\Delta p_s = 0$ hPa, $\Delta T_s = 10$ K; solid red line: $\Delta p_s = 10$ hPa, $\Delta T_s = 10$ K.

vertical temperature lapse rate (Fig. 1c). In this case Δp_C depends on differences in surface pressure and temperature as well as on the lapse rate.

We consider a hydrostatic atmosphere with a constant lapse rate $\Gamma \equiv -\partial T/\partial z$, where pressure and temperature depend on height z and one horizontal coordinate y (Makarieva et al., 2015c):

$$p(y, z) = p_s(y) \left[\frac{T(y, z)}{T_s(y)} \right]^{1/c} \equiv p_s(y) \left[1 - \frac{\Gamma z}{T_s(y)} \right]^{1/c}, \quad (6)$$

$$T(y, z) = T_s(y) - \Gamma z, \quad c \equiv \frac{\Gamma}{\Gamma_g}, \quad \Gamma_g \equiv \frac{Mg}{R}. \quad (7)$$

Subscript s denotes values of pressure and temperature on the geopotential surface; y represents distance along the meridian ($y \equiv a\varphi$, $a = 1$ is the Earth's radius, φ is latitude). When the air moves from y_1 to y_2 following a streamline $z = z(y)$, kinetic energy generation, as follows from Eqs. (1) and (3), is given by

$$A = -RT \int_{y_1}^{y_2} \frac{1}{p(y, z)} \frac{\partial p(y, z)}{\partial y} \Big|_{z=z(y)} dy. \quad (8)$$

Consider a cycle with positive total work as in Fig. 1c. Given the small relative changes of surface pressure and temperature we can write their dependence on y in the linear form:

$$p_s(y) = p - \Delta p_s \frac{y}{\Delta y}, \quad T_s(y) = T + \Delta T_s \frac{y}{\Delta y}, \quad (9)$$

where $p \equiv p_A$, $T^+ \equiv T_A$, $y_A = 0$, $y_{B'} = y_B = \Delta y$, $\Delta p_s > 0$, $\Delta T_s > 0$.

Streamline equations for the warmer isotherm AB with temperature T^+ and the colder

isotherm CD with temperature T^- are obtained from Eqs. (9) and (7):

$$\text{AB : } z(y) = \frac{\Delta T_s}{\Gamma} \frac{y}{\Delta y}; \quad (10)$$

$$\text{CD : } z(y) = z^- + \frac{\Delta T_s}{\Gamma} \frac{y}{\Delta y}, \quad z^- \equiv \frac{T^+ - T^-}{\Gamma}. \quad (11)$$

Differentiating Eq. (6) over y for constant z and using Eqs. (9)-(11) we obtain from Eq. (8) the following expressions for kinetic energy output A^+ and A^- at the warmer and colder isotherms, respectively:

$$A^+ = RT^+ \left[\int_0^{\Delta p_s/p} \frac{dx}{1-x} - \frac{1}{c} \int_0^{\Delta T_s/T^+} \frac{x dx}{1+x} \right], \quad (12)$$

$$A^- = RT^- \left[-\frac{A}{RT^+} + \frac{1}{c} \int_0^{\Delta T_s/T^+} \left(\frac{T^+}{T^-} - 1 \right) \frac{dx}{1+x} \right]. \quad (13)$$

As we will discuss in greater detail below, relative differences $\Delta p_s/p_s$ and $\Delta T_s/T_s$ on Earth possess small magnitudes of the order of $\Delta p_s/p_s \sim 10^{-2}$ and $(1/c)(\Delta T_s/T_s)^2 \sim 10^{-2}$. Therefore, all calculations in Eqs. (12) and (13) can be done to the accuracy of the linear terms over $\Delta p_s/p$ and linear and quadratic terms over $\Delta T_s/T^+$. Performing integration in Eqs. (12) and (13) and expressing the result in these approximations we obtain:

$$A^+ = RT^+ \left[\frac{\Delta p_s}{p} - \frac{1}{2c} \left(\frac{\Delta T_s}{T^+} \right)^2 \right], \quad A_C^+ = A^+ + \frac{R\Delta T_s}{c}, \quad (14)$$

$$A^- = -\frac{T^-}{T^+} A^+ + \frac{R(T^+ - T^-)}{c} \frac{\Delta T_s}{T^+}, \quad A_C^- = -\frac{T^-}{T^+} \left(A^+ + \frac{R\Delta T_s}{c} \right), \quad (15)$$

$$A = -R(T^+ - T^-) \ln \left[\frac{1 - \Delta p_s/p}{(1 + \Delta T_s/T^+)^{1/c}} \right] = A_C^+ + A_C^- = A^+ + A^-. \quad (16)$$

Here $A_C^+ \equiv \int_{V_A}^{V_B} p dV$ and $A_C^- \equiv \int_{V_C}^{V_D} p dV$ are the total work outputs on isotherms AB and CD, respectively (italic subscript "C" stands for "Carnot"); $p \equiv p_A$ and $T^+ \equiv T_A$ are surface pressure and temperature at point A, $p - \Delta p_s \equiv p_{B'}$ and $T^+ + \Delta T_s \equiv T_{B'}$ are pressure and temperature at point B'. Eq. (16) can also be obtained from Eq. (5) with use of Eqs. (6) and (7) and noting that $\Delta p_C = p_B - p_A$ and $z_B = \Delta T_s/\Gamma$.

Let us discuss the physical meaning of the obtained expressions. We first note that kinetic energy generation A^+ , A^- and total work A_C^+ , A_C^- on the two isotherms may have different signs. In particular, at the warmer isotherm kinetic energy generation A^+ can be either positive (at small ΔT_s) or negative (at large ΔT_s), while total work A_C^+ is always positive at large $\Delta T_s > 0$, which reflects the fact that at the lower isotherm the gas expands.

For horizontally isothermal surface with $\Delta T_s = 0$ (Fig. 1b) we have $A^+ > 0$ and $A^- < 0$, i.e. kinetic energy generation at the colder isotherm is negative. It means that in the upper atmosphere the air must move in the direction of growing pressure (see Fig. 1d, solid blue line) thus losing kinetic energy. At the beginning of this path (at point C) the air must possess sufficient kinetic energy exceeding $|A^-| = RT^- \Delta p_s/p$ to cover the entire isotherm CD. If the initial store of kinetic energy is insufficient, at a certain point between C and D the kinetic energy becomes zero. Not having reached point D, the air will start moving in the opposite direction under the action of the pressure gradient force. For $T^- = 200$ K and $\Delta p_s = 10$ hPa we have $A^- = -17$ J mol $^{-1}$ or $A^-/M = -570$ J kg $^{-1}$, where $M = 29$ g mol $^{-1}$ is molar mass of air. This corresponds to an air velocity of about $\sqrt{|A^-|/M} \sim 24$ m s $^{-1}$, which is a typical velocity in the upper troposphere. Thus the cycle shown in Fig. 1b is energetically plausible.

Now consider a situation when $\Delta p_s = 0$, but $\Delta T_s > 0$. The relationship between work outputs is reversed: kinetic energy generation is negative at the warmer isotherm, $A^+ < 0$, and positive at the colder isotherm, $A^- > 0$. This is because at all heights, except at the surface, air pressure is higher in the warmer area towards which the low-level air is moving (Fig. 1d, red dashed line). Thus, as before at the colder isotherm, now the air must spend its kinetic energy to overcome the opposing action of the horizontal pressure gradient force at the warmer isotherm. Using a typical value of $\Delta T_s \sim 10$ K in the Hadley cells for $T^+ = 300$ K, $\Gamma = 6$ K km⁻¹ ($2c = 0.35$, see Eq.(7)) from Eq. (14) we obtain $A^+/M = -270$ J kg⁻¹. This means that the necessary velocity the air must possess at the beginning of the warmer isotherm to be able to cover it all from point A to point B is $\sqrt{|A^-|/M} \sim 16$ m s⁻¹. This exceeds the characteristic velocities at circulation cell boundaries in the boundary layer, which are about 8 m s⁻¹ (e.g., Lindzen and Nigam, 1987; Schneider, 2006, Fig. 1a). Since in the lower atmosphere the air must also overcome surface friction, total energy required to move from A to B with $\Delta p_s = 0$ is larger than estimated from Eq. (14).

If the kinetic energy the air possesses is negligible compared to what is needed to move from A to B, the kinetic energy required must be generated on the warmer isotherm. For kinetic energy generation on the warmer isotherm to be positive, $A^+ > 0$, surface pressure and temperature differences Δp_s and ΔT_s must satisfy

$$K \equiv 2c \frac{\Delta p_s}{p} \left(\frac{T^+}{\Delta T_s} \right)^2 > 1. \quad (17)$$

For $T^+ = 250$ K and $\Delta T_s = 50$ K, which characterize the surface temperature differences between the equator and the poles, at $p = 1000$ hPa and $\Gamma = 6.5$ K km⁻¹ ($2c = 0.38$) we find that to satisfy Eq. (17) the surface pressure difference between the equator and the pole Δp_s must exceed 100 hPa. Such a pressure difference on Earth can be found in intense compact vortices like the severest hurricanes and tornadoes; it is an order of magnitude larger than the typical Δp_s in the two Hadley cells (Fig. 2b), which together cover over half of the Earth's surface.

From Eq. (17) we can derive the maximum size of the cell expressed in terms of the absolute magnitudes of surface pressure and temperature gradients $\nabla p_s \equiv \partial p_s / \partial y = -\Delta p_s / \Delta y$, $\nabla T_s \equiv \partial T_s / \partial y = \Delta T_s / \Delta y$:

$$\Delta y \leq L_{\max} \equiv 2c \frac{|\nabla p_s|}{p} \left(\frac{T^+}{\nabla T_s} \right)^2. \quad (18)$$

For the Carnot cycle, the maximum cell size L_{\max} grows with increasing surface pressure gradient and diminishes proportionally to the squared surface temperature gradient. The surface temperature gradient is largely known: it reflects the differential solar heating that makes the pole colder than the equator. Therefore, the key question in deciding about the maximum cell size is what determines the surface pressure gradient.

4 Thermodynamic cycle with rectangular streamlines

In the Carnot cycle, the ΔT_s term in the expression for kinetic energy generation A^+ is quadratic, see Eqs. (14), (17), (18). This results from the dual nature of the relationship. Firstly, ΔT_s determines the mean height of the warmer isotherm via the streamline equation Eq. (10): the greater ΔT_s , the greater the mean height at which the air moves in the lower atmosphere. Secondly, ΔT_s determines a pressure difference that acts as a sink for kinetic energy in the lower atmosphere (see Fig. 1d, dashed line). This pressure difference increases linearly with small ΔT_s and with height. This double effect leads to the negative quadratic term in Eq. (14), which diminishes the rate at which kinetic energy is generated in a heat engine.

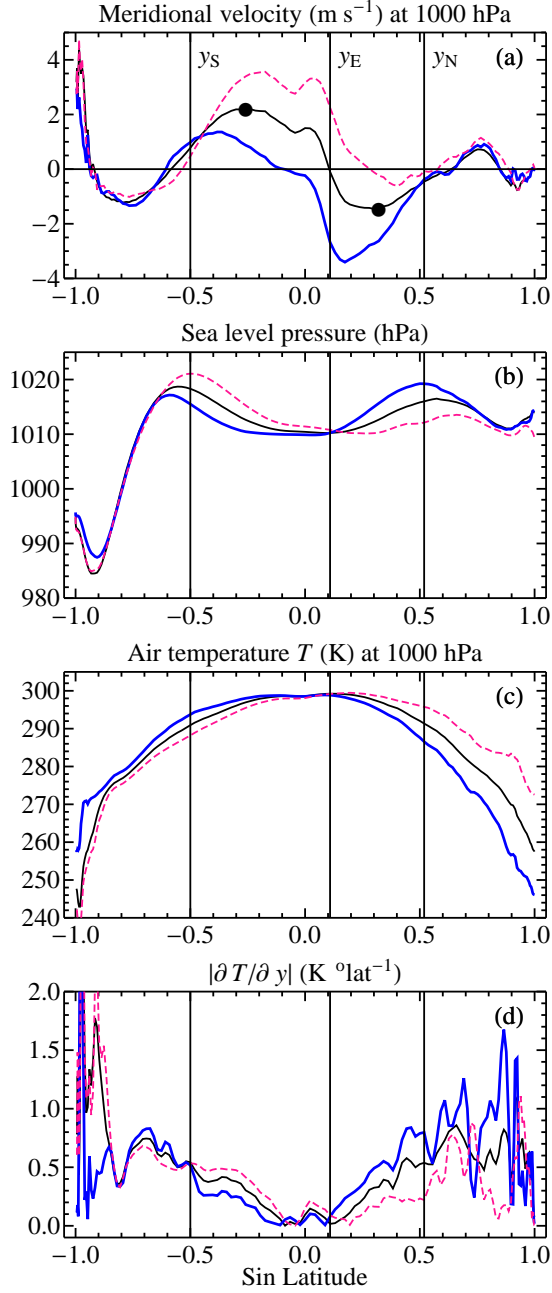


Figure 2: Long-term mean zonally averaged meridional velocity, sea level pressure (SLP), air temperature T at 1000 hPa and its meridional gradient calculated from MERRA data. Black, thick blue and pink dashed curves denote annual mean, January and July data, respectively. Black circles in (a) indicate velocity maxima; y_N , y_S and y_E are the Hadley cell outer and inner borders that are calculated for each of the 432 months from the velocity data (see text for details), here exemplified for the annual mean velocity curve. For each month $\Delta p_{sj} \equiv \text{SLP}(y_j) - \text{SLP}(y_E)$, $\Delta T_{sj} \equiv T(y_E) - T(y_j)$, where $j = S, N$ stand for the Southern and Northern cells, respectively.

We will now consider kinetic energy generation A_r in a cycle where the vertical adiabates are connected by horizontal streamlines. The air moves parallel to the surface at a certain height z that is independent of ΔT_s . It is a cycle with streamlines as shown in Fig. 1b but in the presence of a surface temperature difference as in Fig. 1c.

Using Eqs. (6), (7) and (9) we find that in this case kinetic energy generation at the horizontal streamlines is given by

$$A_r(y_1, y_2, z) = - \int_{p_1}^{p_2} \frac{RT}{p} dp = -R \int_{y_1}^{y_2} \frac{T_s(y) - \Gamma z}{p} \frac{\partial p}{\partial y} dy \quad (19)$$

$$= -R\Gamma z \int_{y_1}^{y_2} \left(-\frac{1}{p_s} \frac{\partial p_s}{\partial y} + \frac{1}{cT_s} \frac{\partial T_s}{\partial y} \right) dy - R \int_{y_1}^{y_2} \frac{T_s}{p_s} \frac{\partial p_s}{\partial y} dy \quad (20)$$

$$= R\Gamma z \ln \left[\frac{1 - \Delta p_s/p}{(1 + \Delta T_s/T^+)^{1/c}} \right] - RT^+ \ln \left(1 - \frac{\Delta p_s}{p} \right) - R\Delta T_s \left[1 + \frac{p}{\Delta p_s} \ln \left(1 - \frac{\Delta p_s}{p} \right) \right]. \quad (21)$$

At the lower AB and upper CD streamlines, kinetic energy generation is calculated from Eq. (21) as follows: $A_r^+ \equiv A_r(y_A, y_B, z^+)$ and $A_r^- \equiv -A_r(y_C, y_D, z^-)$, respectively, where z^+ and $z^- > z^+$ are the altitudes of these streamlines, $y_C = y_B$, and $y_D = y_A$.

Retaining linear terms over $\Delta p_s/p$ and $\Delta T_s/T^+$ (thus discarding the last term in Eq. (21)) for A_r^+ and A_r^- we find

$$A_r^+ = R(T - \Gamma z^+) \frac{\Delta p_s}{p} - R\Gamma z^+ \frac{1}{c} \frac{\Delta T_s}{T^+} = RT \frac{\Delta p_s}{p} - Mg z^+ \frac{\Delta T_s}{T^+}, \quad (22)$$

$$A_r^- = -R(T - \Gamma z^-) \frac{\Delta p_s}{p} + Mg z^- \frac{\Delta T_s}{T^+}, \quad (23)$$

$$A_r \equiv A_r^+ + A_r^- = -R\Gamma(z^- - z^+) \ln \left[\frac{1 - \Delta p_s/p}{(1 + \Delta T_s/T^+)^{1/c}} \right]. \quad (24)$$

We additionally took into account that $\Gamma z^+ \ll T^+$ in the second equality in Eq. (22). Note that $R\Gamma/c = Mg$ (see Eq. (7)).

With $z^+ = \Delta T_s/(2\Gamma)$ equal to the mean height of an isothermal streamline in a Carnot cycle, Fig. 1c, Eq. (22) coincides with Eq. (14): $A^+ = A_r^+$. For the upper streamline Eq. (23) coincides with A^- , Eq. (15), if we put $z^- - z^+ \approx z^- = (T^+ - T^-)/\Gamma$, where $T^+ \equiv T_A$ and $T^- \equiv T_D$, Fig. 1. Under this assumption total work A_r of this cycle coincides with total work of the Carnot cycle, Eq. (16). (It can be shown using Eqs. (6) and (7) that the efficiency of the "rectangular" cycle is lower by a small magnitude of the order of $\Gamma z^+/T$.) As in the Carnot cycle, the contribution of temperature difference ΔT_s to kinetic energy generation is negative at the lower streamline, cf. Eqs. (22) and (14), and positive at the upper streamline, cf. Eq. (23) and (15). But the negative contribution is now linear over ΔT_s , not quadratic.

From Eq. (22) the condition that $A_r^+ > 0$ takes the form

$$A_r^+ = Mgh_s \left(\frac{\Delta p_s}{p} - \frac{z}{h_s} \frac{\Delta T_s}{T^+} \right) > 0, \quad h_s \equiv \frac{RT^+}{Mg}, \quad (25)$$

$$z^+ < z_e \equiv h_s \frac{\Delta p_s}{p} \frac{T^+}{\Delta T_s}. \quad (26)$$

Here h_s is the atmospheric scale height and z_e is the isobaric height at which the pressure difference between two atmospheric columns turns to zero (Makarieva et al., 2015c). Equation (26) indicates that the height where the low-level air moves must be smaller than the isobaric height. Since ΔT_s increases as the cell extends towards the pole, for z^+ to be constant, Δp_s must grow approximately proportionally to ΔT_s . If Δp_s grows more slowly than ΔT_s , then at a certain ΔT_s height z^+ can turn to zero or, at constant z^+ , A_r^+ becomes negative. The dependence between Δp_s and ΔT_s thus dictates the maximum cell size as long as A_r^+ is positive. In Appendices B and C we discuss how Eq. (25) and its implications are impacted by our assumptions of idealized air trajectories and constant lapse rate.

5 Surface pressure, temperature and cell size in Hadley cells

To investigate the dependence between Δp_s and ΔT_s in Hadley cells we used monthly averaged sea level pressure (SLP) and meridional velocity at 1000 hPa from 1979 to 2014 from MERRA re-analysis (a total of 432 months), which has a resolution of $1.25^\circ \times 1.25^\circ$ (144×288 grid cells). For each month we established the long-term mean position of the maxima of zonally averaged SLP at the outer borders of the cells. Then for each month in each year we defined the inner border of the cells y_E as the latitude of minimum zonally averaged SLP located between the long-term maxima (Fig. 2b). SLP values were considered different if they differed by not less than 0.05 hPa. If there were several minimal pressure values equal to each other, we chose the one where the absolute magnitude of the zonally averaged meridional velocity was minimal.

Then for each cell for each month we calculated maximum (by absolute magnitude) velocity poleward from the inner border (Fig. 2a). The outer border of the Northern (N) and Southern (S) cell y_N and y_S was defined as the latitude poleward of maximum meridional velocity where the velocity declined by e times (or changed sign) as compared to the maximum. This relative threshold was chosen because the meridional velocity distributions within the two cells are different: in the Northern hemisphere the seasonal change of meridional velocities is greater than it is in the Southern hemisphere (Fig. 2a). As we are interested in kinetic energy generation that depends on velocity, we need to define the cell borders relevant to velocity. Temperature changes in the regions where velocity is close to zero do not impact the kinetic energy generation.

We find that both in the Northern and Southern cells the dependence between Δp_s and ΔT_s changes with growing ΔT_s . For the Northern cell for the 144 lowest, 144 intermediate and 144 highest values of ΔT_s the linear regression $\Delta p_s = a + b\Delta T_s$ yielded, respectively, $b = 1.03, 0.99$ and 0.09 hPa K^{-1} ; for the Southern cells it was $1.09, 0.60$ and 0.50 hPa K^{-1} (Fig. 3a,b). While for the smaller values of ΔT_s the relationship in both cells is identical and the proportionality coefficient is about 1 hPa K^{-1} , it decreases markedly (in the Northern cell – down to zero) with growing ΔT_s . At constant z^+ this results in declining kinetic energy generation (Eq. (22)).

We further observe that while temperature difference ΔT_s grows with the cumulative extension $L \equiv y_N - y_S$ of the Hadley system, the surface pressure difference reaches a plateau of 17 hPa for $L \approx 64^\circ$ latitude (Fig. 3d,e). Accordingly, for $L < 64^\circ$ the ratio of cumulative pressure and temperature differences for the Hadley system is essentially constant at around 1 hPa K^{-1} , but for larger L it declines by about one third as L grows up to the maximum observed values (Fig. 3f). Figure 4 describes kinetic energy generation A_r^+ at different altitudes in the boundary layer. For $z^+ > 0$ kinetic energy generation declines for $L > 64^\circ$ latitude. For $z^+ = 2$ km A_r^+ becomes zero at the observed maximum extension of the Hadley system $L_{\max} = 72.5^\circ$ latitude.

6 Heat engines and heat pumps

If the poleward extension of a cell with positive total work output (a heat engine like the Hadley cell) is limited, a cell with a negative work output (working as a heat pump) must be present poleward of the heat engine (Fig. 5). This is a requirement of continuity: in the adjacent cells the air must go downwards along the path DA. Hence, in the lower atmosphere the air must move from the warmer to the colder region. Such a heat pump requires an external supply of work, which can be provided by neighboring heat engines that have a positive work output. In the atmosphere of the Earth Ferrel cells are the heat pumps, while the Hadley and Polar cells are the heat engines (see, e.g., Huang and McElroy, 2014).

In the lower atmosphere the global kinetic energy generation for the six cells can be

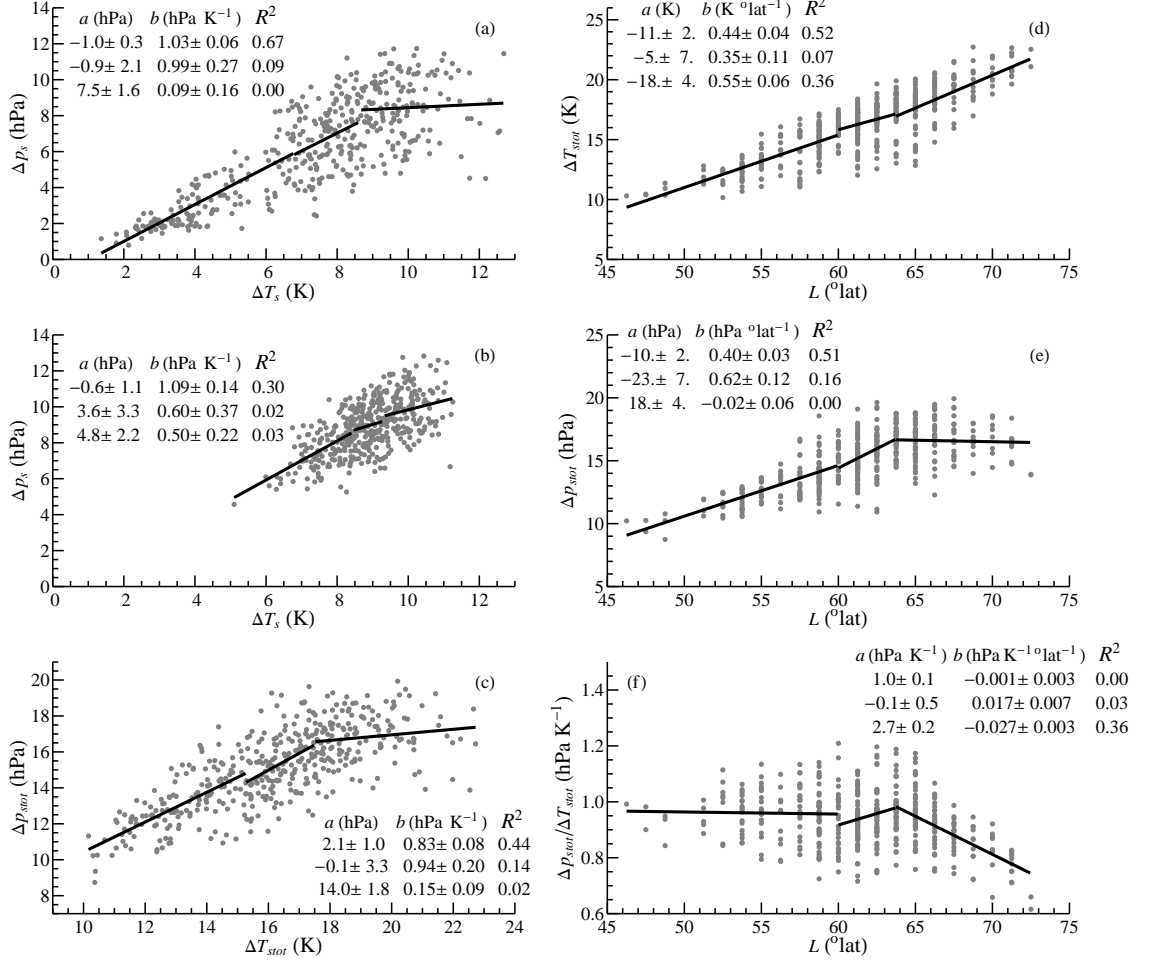


Figure 3: Relationships between surface temperature and pressure differences and the meridional extension of the Hadley system. (a-c): Dependence of Δp_s on ΔT_s in (a) Northern Hadley cell, (b) Southern Hadley cell, (c) Hadley system as a whole: $\Delta p_{stot} \equiv \Delta p_{sN} + \Delta p_{sS} = p_s(y_N) + p_s(y_S) - 2p_s(y_E)$, $\Delta T_{stot} \equiv \Delta T_{sN} + \Delta T_{sS} = T_s(y_N) + T_s(y_S) - 2T_s(y_E)$ (Fig. 2); (d-f): dependence of ΔT_{stot} (d), Δp_{stot} (e) and their ratio (f) on the total extension of the Hadley system ($L \equiv y_N + |y_S|$) (degrees latitude). Solid lines denote linear regressions $y = ax + b$ for the 144 lowest, 144 intermediate and 144 highest values of $x = \Delta T_s$ (a,b), $x = \Delta T_{stot}$ (c) and $x = L$ (d-f). Regression parameters are shown in each panel starting from the lowest x values.

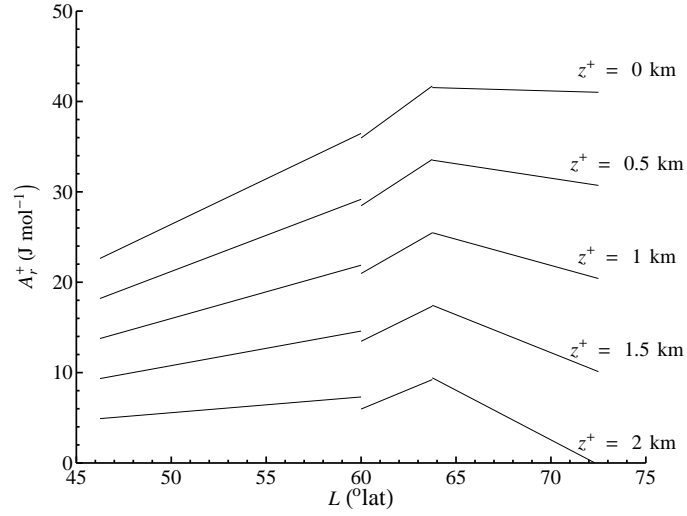


Figure 4: Kinetic energy generation A_r^+ at different altitudes z^+ in the lower atmosphere versus Hadley system size L as determined from Eq. (22) using the observed Δp_{stot} and ΔT_{stot} values from Fig. 3d,e.

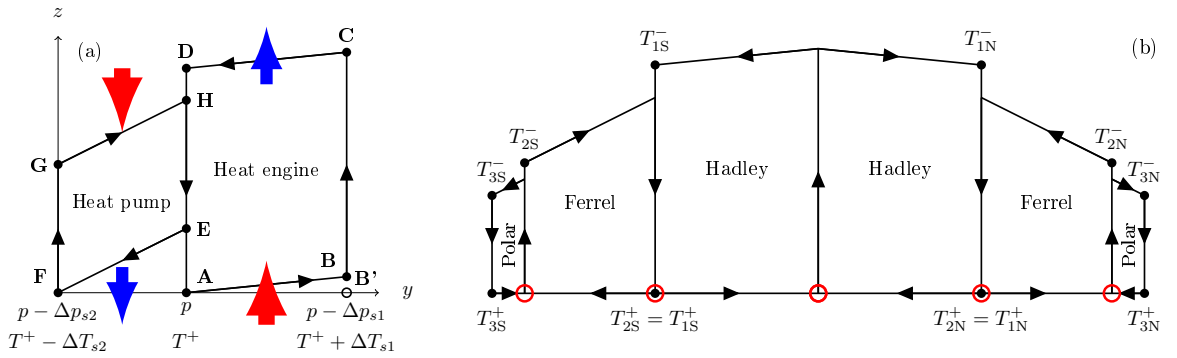


Figure 5: Heat pumps and heat engines. (a) A Carnot heat pump (cycle EFGHE) bordering with a Carnot heat engine (cycle ABCDA). See Fig. 1 for details. (b) The meridional circulation cells on Earth. Arrows show the direction of air movement. Empty red circles indicate the latitude of cell borders as determined in Fig. 6a from meridional velocity values. Black circles indicate where temperature and pressure values used in Eqs. (27) and (28) were calculated. The vertical dimension is height z , the horizontal dimension is sine latitude which accounts for cell area.

Table 1: Contributions of surface pressure and temperature differences to kinetic energy generation for hybrid cycles that have isothermal streamlines in the upper atmosphere (Eq. (15)) and horizontal streamlines in the lower atmosphere (Eq. (22)). (For heat pumps the expression is valid for $\Delta T_s \ll T^+ - T^-$, cf. Eq. (29)).

	Pressure	Temperature	
	All cells	Heat engines	Heat pumps
Upper atmosphere	$-RT^- \frac{\Delta p_s}{p}$	$+\frac{R}{c} \left[(T^+ - T^-) \frac{\Delta T_s}{T^+} + \frac{T^-}{2} \left(\frac{\Delta T_s}{T^+} \right)^2 \right]$	$-\frac{R}{c} \left[(T^+ - T^-) \frac{\Delta T_s}{T^+} + \frac{T^-}{2} \left(\frac{\Delta T_s}{T^+} \right)^2 \right]$
Lower atmosphere	$+RT^+ \frac{\Delta p_s}{p}$	$-Mgz^+ \frac{\Delta T_s}{T^+}$	$+Mgz^+ \frac{\Delta T_s}{T^+}$

written using Eq. (22) as

$$A_g^+ = \sum_{j=S,N} \sum_{i=1}^3 a_{ij} \left[(-1)^i Mgz \frac{\Delta T_{ij}}{T_{ij}^+} + RT_{ij}^+ \frac{\Delta p_{ij}}{p_{ij}} \right]. \quad (27)$$

Here summation is over the six cells, three in the Southern ($j = S$) and three in the Northern ($j = N$) hemisphere, $i = 1, 2, 3$ for Hadley, Ferrel and Polar cells, respectively; $\Delta T_{ij} \equiv \Delta T_{sij} > 0$ and $\Delta p_{ij} \equiv \Delta p_{sij} > 0$ stand for the differences in surface temperature and pressure within the cell; T_{ij} and p_{ij} are surface temperature and pressure at the beginning of the lower streamline (Fig. 5). Note that $T_{1j}^+ = T_{2j}^+$ and $p_{1j}^+ = p_{2j}^+$ (the lower streamlines in Hadley and Ferrel cells start from the same latitude). We have accounted for the area by introducing coefficients $a_{ij} = \sin y_{Pij} - \sin y_{Eij}$, which is the relative area of the cell, where y_P and y_E are the latitudes of cell borders closest to the pole (P) and equator (E) (for Polar cells $y_P = \pm 90^\circ$). Thus work output of each cell is weighted by area.

Coefficient $(-1)^i$ differentiates heat engines ($i = 1, 3$) from heat pumps ($i = 2$) (Table 1). For a "rectangular" heat pump where low surface pressure is associated with low surface temperature, such that the air compresses at the lower streamline, the temperature terms in Eqs. (22) and (23) change their sign. (Note that the pressure terms do not change their sign if, as in the heat engine, the low level air moves from high to low surface pressure.) In a heat pump the temperature difference makes a negative contribution to kinetic energy generation in the upper atmosphere and a positive contribution in the lower atmosphere (Table 1). Thus kinetic energy generation in the lower atmosphere can be expected to be greatest in heat pumps, which agrees with observations (see Table 2 below).

To estimate global kinetic energy generation in the upper atmosphere we use Eq. (15) for the colder isotherm of the Carnot cycle (Fig. 5b):

$$A_g^- = \sum_{j=S,N} \left[\sum_{i=1,3} a_{ij} A_{ij}^- + a_{2j} A_{2j}^- \right], \quad (28)$$

$$A_{2j}^- = -RT_{2j}^- \left[\frac{\Delta p_{2j}}{p_{2j}} + \frac{1}{2c} \left(\frac{\Delta T_{2j}}{T_{2j}^+} \right)^2 \right] - R(T_{2j}^+ - \Delta T_{2j} - T_{2j}^-) \frac{1}{c} \frac{\Delta T_{2s}}{T_{2j}^+}. \quad (29)$$

Here A_{ij}^- for $i = 1, 3$ is work output of the heat engines (Polar and Hadley cells), Eq. (15); $A_{2j}^- < 0$ is work output of the heat pumps (Ferrel cells)¹. It can be obtained following the procedure that yielded Eq. (15) but for the isotherm GH instead of CD (Fig. 5a).

¹Note that Eq. (29) is not completely symmetrical to Eq. (15), because in a heat pump temperature of the warmer isotherm T_{2j}^+ is not equal to surface temperature $T_{2j}^+ - \Delta T_{2j}$ at the beginning of the warmer isotherm (which is point E in Fig. 5a). Meanwhile in the heat engine (ABCD) temperature of the warmer isotherm coincides with surface temperature at point A.

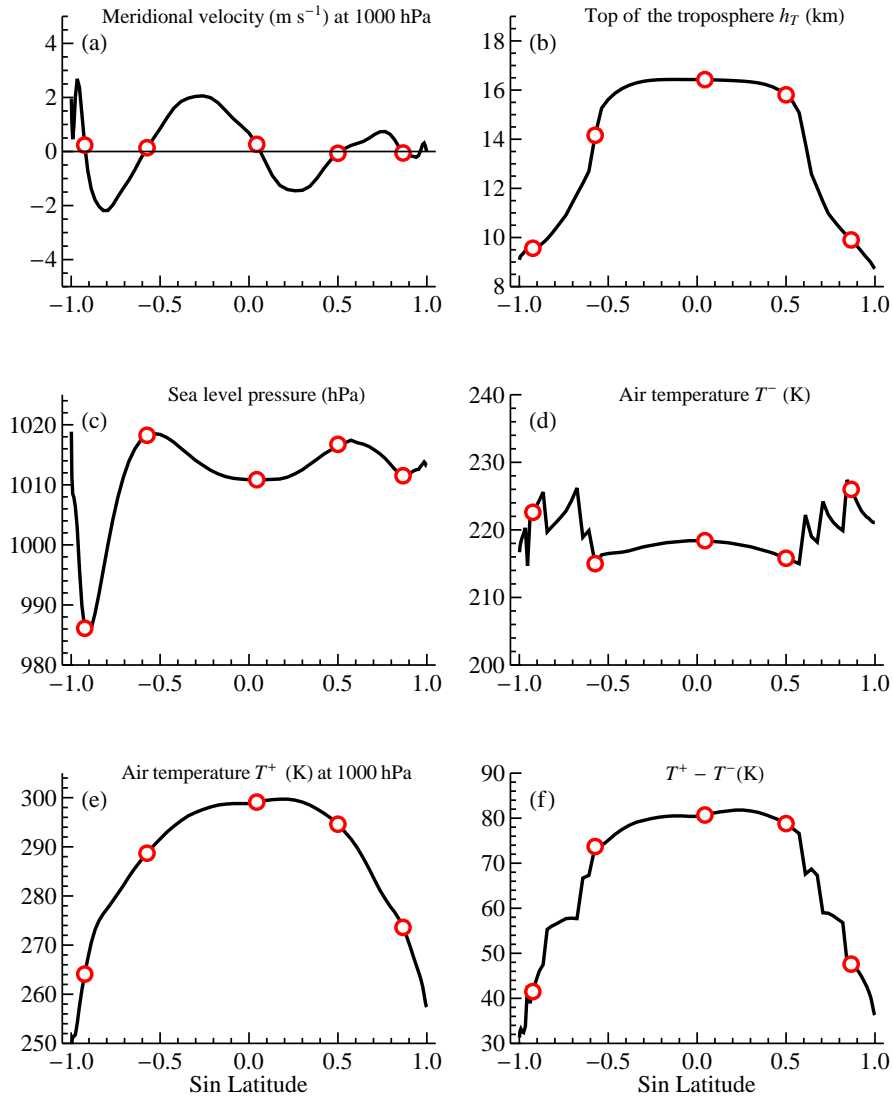


Figure 6: Annual mean values of parameters used in Eqs. (27) and (28) to calculate global kinetic energy generation. Empty red circles denote cell borders defined in (a) as the points where meridional velocity changes sign (see also Fig. 5b).

To explore how expressions (27) and (28) relate to observations we used NCAR/NCEP monthly re-analyses data (averaged over the period from 1979-2013) on sea level pressure, geopotential height and air temperature at 13 pressure levels provided by the NOAA/OAR/ESRL PSD, Boulder, Colorado, USA, from their Web site at <http://www.esrl.noaa.gov/psd/> (Kalnay et al., 1996). All data were zonally averaged. We defined the cell borders as positions where the zonally averaged meridional velocity at 1000 hPa changes its sign (Fig. 6a). We approximated T_{ij}^- as the temperature of the top of the troposphere, having defined the latter, following Santer et al. (2003), as the height where the lapse rate diminishes to 2 K km^{-1} .

In Fig. 6 we show the height of the troposphere h_T , cell borders, and temperatures for the Northern and Southern hemispheres. We can see that T^- is relatively constant across the cells (Fig. 6d), while the height of the troposphere (which is a proxy for cell height z^-) decreases twofold within the Ferrel cells (Fig. 6b). This justifies the use of the Carnot formula for A^- , i.e. Eq. (15) rather than Eq. (23) for the horizontal streamline, to describe the upper streamline in the real cells. The results are shown in Table 2.

For the lower atmosphere we find that total kinetic energy generation of $A_g^+ = 55 \pm$

Table 2: Budget of kinetic energy generation (J mol^{-1}) calculated from Eqs. (27) and (28) for the heat engines (Hadley and Polar cells) and heat pumps (Ferrel cells) (Northern and Southern hemispheres combined) for $z^+ = 1 \text{ km}$ and $c = 0.19$ ($\Gamma = 6.5 \text{ K km}^{-1}$). Uncertainty represents the standard deviation for monthly variation. "Total" in the last column includes the $(\Delta T_s/T^+)^2$ contribution from the upper atmosphere (this term is absent in the lower atmosphere).

	Lower atmosphere			Upper atmosphere				Lower and upper atmosphere		
	Total	$\Delta p_s/p$	$\Delta T_s/T^+$	Total	$\Delta p_s/p$	$\Delta T_s/T^+$	$(\Delta T_s/T^+)^2$	$\Delta p_s/p$	$\Delta T_s/T^+$	Total
Ferrel	44 ± 5	30 ± 4	14 ± 2	-152 ± 23	-23 ± 3	-111 ± 17	-18 ± 4	7 ± 2	-97 ± 16	-108 ± 18
Hadley	9 ± 1	20 ± 2	-11 ± 1	108 ± 11	-15 ± 1	116 ± 11	7 ± 1	5 ± 1	105 ± 10	117 ± 11
Polar	2 ± 2	6 ± 3	-4 ± 2	19 ± 4	-5 ± 3	18 ± 4	6 ± 4	0.7 ± 0.3	14 ± 4	21 ± 4
All cells	55 ± 6	56 ± 5	-1 ± 3	-25 ± 23	-43 ± 3	23 ± 18	-5 ± 7	13 ± 2	22 ± 16	30 ± 19

6 J mol^{-1} is determined by surface pressure differences, which make positive contributions to A_g^+ in all cells. The contribution of the temperature term is virtually zero, for $z^+ = 1 \text{ km}$ (boundary layer) in Eq. (27) it constitutes $-1 \pm 3 \text{ J mol}^{-1}$. The absolute magnitude of the contributions of ΔT_s within individual cells is substantially smaller than that from Δp_s : it is positive in Ferrel cells and negative in Hadley cells, contributing about 20% of A_g^+ by absolute magnitude.

The mean kinetic energy generation by the upper atmosphere is negative, $A_g^- = -25 \pm 23 \text{ J mol}^{-1}$. Surface pressure differences make negative contributions in all cells, while the surface temperature contributions are positive in some cells, i.e. the Hadley and Polar cells as heat engines, and negative in others, i.e. the two Ferrel cells as heat pumps. The linear temperature term is also the most variable: this variability is both spatial and temporal reflecting seasonal migration of cell borders.

Global kinetic energy generation is given by $A_g \equiv A_g^+ + A_g^- = 30 \pm 19 \text{ J mol}^{-1}$, which is 25% of what is generated by the Hadley system ($A_H = 117 \pm 11 \text{ J mol}^{-1}$). This is consistent with the analysis of Kim and Kim (2013) who found that the net global meridional kinetic power W_g in NCAR-NCEP re-analysis is slightly positive, albeit different methods of calculations gave different results: $W_g = 0.06 \text{ W m}^{-2}$ or 0.10 W m^{-2} . Assuming that the Hadley system contributes $198 \times 10^{12} \text{ W}$ (Huang and McElroy, 2014) or $W_H = 0.4 \text{ W m}^{-2}$ globally, we conclude that in the NCAR-NCEP re-analysis the net meridional kinetic power is 15-25% of the kinetic power in the Hadley system. This is in agreement with our results that are based on NCAR-NCEP data: $W_g/W_H = A_g/A_H$ obtained from Eqs. (27) and (28) (Table 2). (Note that an equality between the ratios of power W_i (W) and work A_i (J mol^{-1}) in different circulation systems implies an equality between the amounts of gas \mathcal{N}_i/τ_i circulating per unit time along the considered streamline in each system: $W_i = A_i \mathcal{N}_i/\tau_i$, where \mathcal{N}_i (mol) is the number of moles circulating along the considered streamline in the i -th circulation, τ_i is the time period of the cycle.) In the MERRA re-analysis the net meridional kinetic power is slightly negative: $W_g = -0.06 \text{ W m}^{-2}$ or -0.13 W m^{-2} (Kim and Kim, 2013). According to MERRA, the Ferrel cells consume more kinetic power than the Hadley cells produce (Huang and McElroy, 2014). The pattern common to both datasets is that most kinetic energy generated by the heat engines is consumed by the heat pumps. This robust pattern is reproduced by our analysis (Table 2).

7 Discussion and conclusions

7.1 Kinetic energy generation as a function of surface pressure and temperature differences

We derived how kinetic energy generation in the boundary layer, A^+ and A_r^+ , and in the upper atmosphere, A^- and A_r^- , depends on surface pressure and temperature differences Δp_s and ΔT_s that are measured along the air streamline. This derivation is based on three fundamental relationships: the hydrostatic equilibrium, the ideal gas law and the definition of mechanical work of an air parcel. The obtained expressions are valid for any air parcel following a given trajectory irrespective of the angular velocity of planet rotation.

We applied the derived relationships to analyze kinetic energy generation in Earth's meridional circulation cells. On Earth a typical meridional surface temperature difference ΔT_s makes a larger contribution to total kinetic energy generation A than a typical surface pressure difference Δp_s . E.g., for a Hadley cell $(1/c)\Delta T_s/T \approx 10\Delta p_s/p \approx 0.1$. Kinetic energy generation by a temperature-induced pressure gradient in the upper atmosphere is by a similar factor larger than kinetic energy generation by the surface pressure gradient at the lower isotherm, $A^- \gg A$, Eqs. (14)-(15). These relationships might have been responsible for the lack of explicit attention to surface pressure gradients when considering the atmospheric thermodynamic cycles and kinetic energy budget.

However, as we have shown, the surface temperature gradient plays a two-sided role. Firstly, it generates a pressure gradient in the upper atmosphere, which can be a source of kinetic energy. Secondly, the same pressure gradient, if the air moves from the colder to the warmer region, consumes kinetic energy. Such a "negative" cycle (heat pump) must be fed by a "positive" cycle (heat engine) that has a positive work output. Therefore, in the presence of a surface temperature gradient along which several circulation cells are operating, the global efficiency of kinetic energy generation can never reach Carnot efficiency: the circulation cells with negative work output can reduce it to zero. A global Carnot efficiency for an atmosphere containing many circulation cells can be achieved only on an isothermal surface where all cells are represented by Carnot cycles shown in Fig. 1b ($\Delta p_s > 0$, $\Delta T_s = 0$, $A > 0$).

7.2 Small net kinetic energy generation in the upper atmosphere

Our analytical formulations permit us to quantify the relative magnitudes of the surface pressure and temperature contributions to kinetic energy generation. We show that because of the large negative surface temperature differences across the Ferrel cells, these cells consume most of the kinetic energy generated by the Hadley cells in the upper atmosphere (Table 2). This is consistent with observations of the Ferrel and Hadley systems (see Huang and McElroy, 2014; Kim and Kim, 2013).

Our simplified analysis does not permit us to estimate the net kinetic energy generation in the upper atmosphere with high precision. However, our inspection of the up-to-date analysis of atmospheric kinetic power reveals that the kinetic energy sources and sinks in the upper atmosphere virtually cancel each other out. Huang and McElroy (2015) recently performed a high-resolution analysis of global kinetic power generation using 3-hour $1.25^\circ \times 1.25^\circ$ gridded MERRA data (such an analysis obviously accounts for both eddy and zonally averaged components of the circulation). These data, reproduced in Fig. 7, show that in the lower atmosphere kinetic power is almost universally positive, while in the upper atmosphere there are large sources and sinks of kinetic energy that are in approximate balance. The net kinetic energy generation in the upper atmosphere appears to be small compared to the lower atmosphere².

²We emphasize that the local rate of kinetic energy generation in the upper atmosphere can be significantly higher than it is on average in the lower atmosphere, cf. Fig. 3b and 3c of Huang and McElroy (2015). Thus the small net value does not reflect a ubiquitous geostrophic balance (under geostrophic

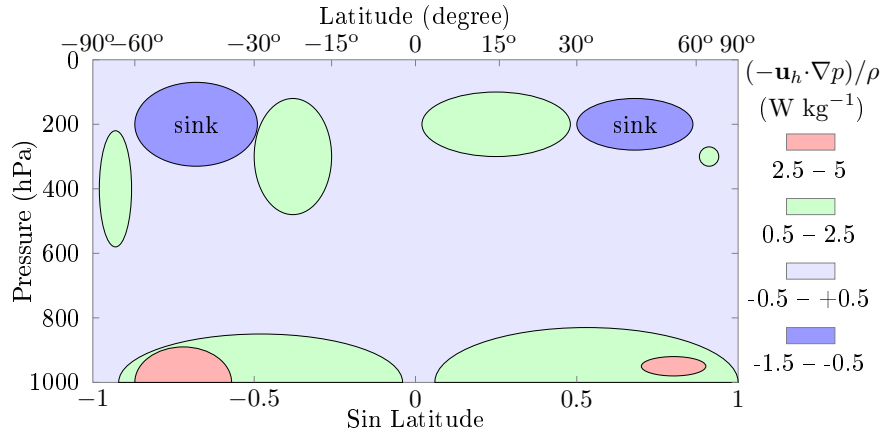


Figure 7: Schematic representation of the budget of kinetic power generation in the upper and lower atmosphere redrawn from Fig. 3a of Huang and McElroy (2015). Note sinks of kinetic energy in the upper parts of the Ferrel cells.

To our knowledge, this remarkable pattern – the cancellation of large energy sources and sinks in the upper atmosphere – has not been previously noted. Negligible kinetic energy generation in the upper atmosphere means that the positive temperature contribution of circulation cells that work as heat engines must compensate the negative temperature contribution of all heat pumps as well as the negative pressure contribution in both heat pumps and heat engines (Table 1). Given that these contributions are governed by several independent parameters, including surface pressure, temperature, lapse rate, height and width of the circulation cell, a random combination of these terms resulting in a small net kinetic energy generation appears unlikely. In our view, this compensation results from a dynamic constraint which determines that the export/import of kinetic energy from/to the upper atmosphere is small. For a given distribution of surface pressure and temperature, this condition can be satisfied by varying the height z^- and temperature T^- of the upper streamlines that determine kinetic energy generation and its consumption in the upper troposphere (Table 1). In other words, the observed height of the troposphere as well as the isobaric height (26) can be determined by the condition that net kinetic energy generation in the upper atmosphere is small. We suggested previously that rather than determining the ratio between surface pressure and temperature differences (Lindzen and Nigam, 1987; Bayr and Dommenges, 2013), these heights likely result from these differences (Makarieva et al., 2015c).

When kinetic energy generation in the upper atmosphere is negligible, global kinetic energy generation is determined by surface pressure gradients. The temperature contribution in the lower atmosphere is relatively small due to the small factor $z^+/h_s < 0.1$ (see Eqs. (25) and (36)).

7.3 The role of surface pressure gradients and condensation

The obtained expressions for A_r^+ and A^- show that in the upper atmosphere kinetic energy generation grows with increasing ΔT_s , while in the lower atmosphere it declines. For a circulation cell where the air moves towards a warmer area, this means that the larger the temperature difference between the warm and the cold ends of the cell, the less kinetic energy is generated in the boundary layer. This explains, for example, why maximum kinetic energy in the lower atmosphere is generated within Ferrel cells, where ΔT_s is minimal (i.e. where $\Delta T_s < 0$ as the surface air moves towards a colder area, see Table 2 and Fig. 7.)

balance kinetic energy generation would be zero everywhere).

As the pole is colder than the equator, the temperature difference ΔT_s across the meridional circulation cell grows with increasing meridional cell extension L . The obtained theoretical expression for A_r^+ shows that if the surface pressure difference Δp_s remains constant, A_r^+ will decrease linearly with growing L . In such a case the condition that A_r^+ in the boundary layer must be positive will limit the cell size. Using monthly MERRA data, we showed that for the real-world Hadley cells ΔT_s does indeed grow with L , but that Δp_s reaches a plateau at some intermediate values of L beyond which it does not further grow with increasing L despite increasing ΔT_s . This means that there is a maximum value of kinetic energy that can be generated in the lower atmosphere in Hadley cells (Fig. 4).

The work performed by the turbulent friction force at the surface grows with increasing cell size (and hence increasing streamline length). Since generation and dissipation of kinetic energy must balance each other, this means that kinetic energy generation in the boundary layer cannot be less than a certain positive value corresponding to friction losses. Other things being equal, if surface friction losses are reduced, the poleward cell extension can grow, an effect noted by Robinson (1997). Meanwhile in the upper atmosphere, as noted in many studies (e.g., Held and Hou, 1980; Robinson, 1997; Marvel et al., 2013), friction has an opposite effect on cell size: the poleward cell extension grows with *increasing* turbulent friction (eddy diffusivity) in the atmospheric interior (because of a smaller degree of momentum conservation in the upper level flow as discussed in the Introduction).

Surface pressure gradients have been traditionally considered as outcomes of air redistribution in the upper atmosphere caused by temperature gradients (e.g., Pielke, 1981). In terms of the energy budget of a thermodynamic cycle, this can be understood as follows. A certain part of kinetic energy generated in the upper atmosphere in a heat engine is not consumed by heat pumps but is converted to the potential energy of the surface pressure gradient. This potential energy then is converted to the kinetic energy as the air moves in the boundary layer. This explanation would be valid for the real Earth if we could show from theory that the upper-level air flow along the observed temperature gradients do indeed generate enough potential energy to form a surface pressure gradient of observed magnitude. However, since the upper level air flow and, hence, kinetic energy generation in the upper atmosphere, can only be found by explicitly specifying turbulent friction, which is not known from theory, the question as to what determines surface pressure gradients across the meridional cells remains open. (We note that whatever is the cause of the surface pressure gradients apparently they do not always grow with increasing ΔT_s .)

As discussed in the introduction, the presence of the meridional temperature gradient alone is insufficient to generate a meridional circulation of appreciable intensity and poleward extension. Some mechanism (like turbulence) must break the geostrophic equilibrium and allow the upper-level air to actually move towards the pole. Only in such a case there appears a heat engine that could generate some kinetic energy. If we start from the observation that in the tropical upper troposphere there is a poleward air motion (which means that the geostrophic balance is broken), we implicitly provide such a mechanism – however without explaining its nature. Then the properties of the low-level flow, including the surface pressure gradient, can be deduced and understood from the conservation of mass and angular momentum as illustrated by both theory and observational analyses (e.g., Johnson, 1989; Cai and Shin, 2014). If, on the other hand, we start from the observed pressure gradient and the intensity of air motion in the boundary layer, using the same conservation laws we can deduce the upper-level air motions. However, as such diagnostic studies do not investigate the causes of the dynamic disequilibrium that makes the meridional circulation possible and define its intensity in the lower and upper atmosphere, they do not identify the primary drivers of atmospheric circulation.

The explanation of surface pressure gradients as outcomes of temperature gradients is certainly valid for a dry atmosphere where no other sources of potential energy for a surface pressure gradient can be thought of. However, in a moist atmosphere there is a different process that directly impact surface pressure: condensation and precipitation. In the Earth's

atmosphere the instantaneous rates of condensation, which is proportional to vertical velocity, can be two orders of magnitude greater than the instantaneous rates of evaporation. Rapid removal of large amounts of water vapor necessarily disturbs whatever balance of forces might have existed at the surface. The air converges towards this zone of low pressure. Therefore, in a moist atmosphere that is unstable to condensation, a geostrophic equilibrium and, thus, zero rate of kinetic energy generation are principally impossible. If condensation continuously disturbs the geostrophic balance of a rotating atmosphere, the power of the global atmospheric engine should be proportional to condensation rate (see also Makarieva et al., 2013b,a, 2014). Establishing a link between the wind power and condensation implies the need to revise how turbulent friction is formulated in global circulation models.

Let us conclude by highlighting some implications of these mechanisms. Kinetic power generation governed by the product of horizontal velocity and pressure gradient reflects cross-isobaric motion towards the low pressure area and the associated air convergence. If the kinetic power generation is proportional to condensation rate, then over a dry continent where condensation is absent low-level air convergence will be strongly suppressed, and a geostrophic (or cyclostrophic) balance will be established. The low pressure area over a dry hot land will not lead to moisture convergence from the ocean, and drought will persist. This indicates that removal of forest cover which is a significant store and source of moisture on land can lead to a self-perpetuating drought. This mechanism may contribute to the recent major shifts in global rainfall patterns like for example the recent catastrophic droughts in Brazil (Marengo and Espinoza, 2015; Dobrovolski and Rattis, 2015).

We urge increased attention to the nature of surface pressure gradients on Earth and the role of condensation in their generation.

8 Acknowledgment

This work is partially supported by Russian Scientific Foundation Grant 14-22-00281, the University of California Agricultural Experiment Station, the Australian Research Council project DP160102107 and the CNPq/CT-Hidro - GeoClima project Grant 404158/2013-7.

Appendix A. Work in the presence of phase transitions

Here we show that Eq. (3) accurately describes kinetic energy generation even in the presence of phase transitions. Consider an air parcel occupying volume $\tilde{V} \equiv \tilde{N}V$ and containing a total of $\tilde{N} = \tilde{N}_d + \tilde{N}_v$ moles of dry air and water vapor (subscript d and v , respectively). This air parcel moves along a closed stationary trajectory which can be described in (p, V) coordinates (e.g. Fig. 1a). Total work performed by such an air parcel per mole dry air is

$$A_p \equiv \frac{1}{\tilde{N}_d} \oint p d\tilde{V} = \frac{1}{\tilde{N}_d} \left(\oint \tilde{N} p dV + \oint p V d\tilde{N} \right), \quad \oint d\tilde{N} = 0. \quad (30)$$

Here $d\tilde{N} = d\tilde{N}_v$ is the change of air amount due to phase transitions of water vapor. Unlike A in Eq. (3), A_p (subscript p refers to the presence of phase transitions) is not a unique function of the integral $\oint p dV$ that is determined by the area enclosed by the closed streamline in the (p, V) diagram: A_p additionally depends on where along this trajectory the phase transitions take place. This information is absent from the p, V diagram.

Using the ideal gas law (1), the hydrostatic equilibrium (2) and taking into account that $\oint d(\tilde{N}_v T) = \oint d(\tilde{N} T) = \tilde{N}_d \oint dT = 0$, we find

$$A_p = -\frac{1}{\tilde{N}_d} \oint \tilde{N} V dp = -\frac{1}{\tilde{N}_d} \oint \tilde{N} V \left(\frac{\partial p}{\partial y} \Big|_{z=z(y)} dy + \frac{\partial p}{\partial z} \Big|_{y=y(z)} dz \right) \quad (31)$$

$$= -\oint (1 + \gamma_d) V \frac{\partial p}{\partial y} \Big|_{z=z(y)} dy + \frac{1}{\tilde{N}_d} \oint \tilde{N} M g dz. \quad (32)$$

Here $\gamma_d \equiv \tilde{N}_v / \tilde{N}_d \ll 1$. The second integral in Eq. (32) reflects the difference between the air mass $\tilde{N} M$ (kg) that is rising ($dz > 0$) and descending ($dz < 0$) along the trajectory. This difference is caused by phase transitions (condensation and evaporation) that in the general case occur at different heights z . Therefore, the second integral in Eq. (32) represents the difference in potential energy per mole dry air between the mean heights where condensation and evaporation take place. It is unrelated to the kinetic energy generation (for further details see Makarieva et al., 2015a,b).

We conclude that in the presence of phase transitions, total work output A_p is not equal to kinetic energy generation because of the non-zero second integral in Eq. (32), $A_p \neq A$. However, the kinetic energy generation, which depends on the horizontal pressure gradient and is described by the first integral in Eq. (32), coincides with A (3) with good accuracy because of the small value of $\gamma_d \ll 1$.

Appendix B. Validity of the theoretical approach

Our derivations have assumed an atmosphere with a constant lapse rate and idealized air trajectories. We now examine how these assumptions impact our two major findings: first, how maximum cell size depends on surface pressure and temperature differences, Eqs. (17) and (26); second, our conclusion that in the meridional cells the balance between kinetic energy generated by heat engines and consumed by heat pumps reflects the meridional differences in surface temperature (Table 1 and 2).

The first finding is based on the expression for kinetic energy generation in the lower atmosphere: A^+ (Eq. (14)) for Carnot and A_r^+ (Eq. (22)) for the rectangular cycle. Since A_r^+ is linear over Δp_s , ΔT_s and z (height of air motion), Eq. (22) with $z = \bar{z}$ can be applied to any trajectory of air motion with a sufficiently small mean height \bar{z} . This is because even if the lapse rate Γ varies in the horizontal and/or vertical, the smallness of \bar{z} will ensure that $T(\bar{z}) \approx T^+$ (air temperature is approximately equal to surface temperature) in the pressure term in Eq. (22). For $z = 1$ km and a typical tropical ratio $\Delta p_s/p \sim (1/3)\Delta T_s/T$ (Lindzen and Nigam, 1987; Bayr and Dommenges, 2013; Makarieva et al., 2015c), the pressure term is the main one determining the value of A_r^+ (22). In 8 we discuss that any possible impact of the spatial variation in lapse rate is also negligible.

As we show in Fig. 8, most kinetic energy in the lower half of the troposphere is generated within a narrow boundary layer: the rate of kinetic energy generation diminishes linearly with increasing altitude approaching zero for $z \approx 2$ km (the Northern Ferrel cell is an exception discussed below). If within this layer the distribution of air pressure is satisfactorily described by Eq. (6) with a constant lapse rate, then our formula for kinetic energy generation in the lower atmosphere A_r^+ , Eq. (22), is valid (in calculations in Table 2 we used $z = 1$ km). Indeed, Fig. 8a,b shows that in the Hadley cells in the lowest 2 km the observed pressure difference across the cell is very close to the theoretical pressure difference calculated from Eq. (6). The reason is that the pressure scale height h_s (25) is governed by surface temperature, such that whatever the differences there are in the lapse rates, given

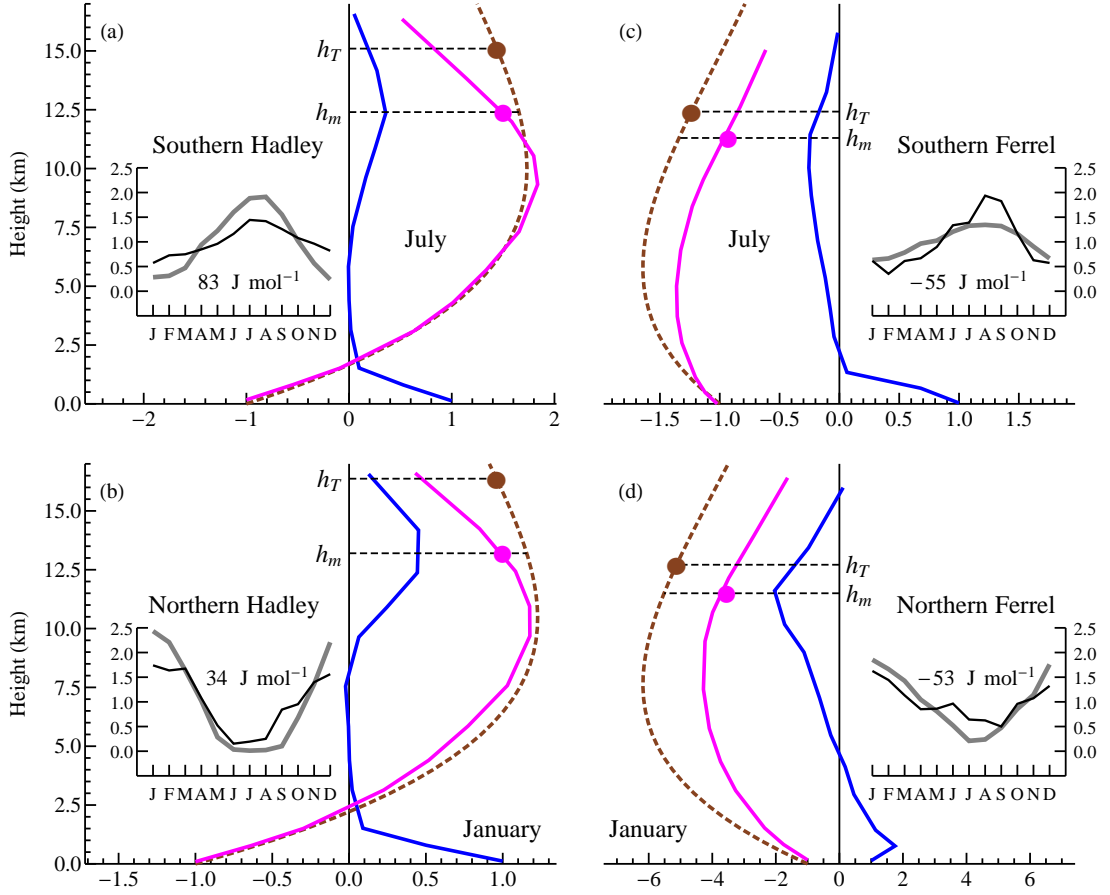


Figure 8: Vertical profiles of the observed (solid pink) and theoretical (dashed brown) pressure differences $\Delta p(z)$ (cf. Fig. 1d) between the borders of (a) Southern Hadley cell in July, (b) Northern Hadley cell in January, (c) Southern Ferrel cell in July, (d) Northern Ferrel cell in January. During these months the cells have the maximum power output (see the insets, see key below). The blue curves indicate estimated kinetic power generation: the product of the mean meridional pressure gradient within the cell by the mean meridional velocity as dependent on height z as a proxy measure. All vertical profiles are normalized by their value at the surface. The small filled circles denote the theoretical pressure difference at the top of the troposphere $z = h_T$ (mean h_T within the cell is shown) and the observed pressure difference at $z = h_m$, the height where kinetic energy generation in the upper troposphere is maximum. The data are long-term mean NCEP-NCAR climatology (see Section 6). The insets show the monthly variation of the theoretical work output for each cell (thin black lines), Eqs. (27), (28), compared to the monthly variation of the observed power output in the same cell (thick gray lines) according to the data of Fig. 2 and 7 of Huang and McElroy (2014). The monthly values are normalized by the annual mean (for the work output the annual mean value is shown on the graph).

z is small, they cannot significantly change this basic height in the boundary layer. Any effect of the actual form of the air trajectory or of variations in lapse rate in time and space will be negligible. We thus conclude that Eqs. (22) and (26) for the rectangular cycle are always valid for the Hadley cells.

Note that in the Northern Ferrel cell the generation of kinetic energy is not confined to the lower 2 km of the atmosphere (presumably because this cell harbors most land including mountains) (Fig. 8c). In this cell our theoretical relationship apparently overestimates the observed pressure difference already in the lower troposphere. However, the two inaccuracies partially cancel each other in our estimate in Table 2: the mean height where kinetic energy is generated in the lower part of the Northern Ferrel cell is approximately twice the value of $z = 1$ km that we assumed for all cells; but the observed pressure difference at this height is about 1.5 times lower than the theoretical pressure difference (Fig. 8c).

The relationships for the Carnot cycle in the lower atmosphere, Eqs. (14) and (17), presume that the mean height of the lower streamline is proportional to ΔT_s . In the real cells the mean height of the low-level air trajectory does not vary linearly with ΔT_s . The Carnot relationships have a theoretical value: they explain how because of the heat pumps an ideal Carnot efficiency in the atmosphere as a whole can be unachievable in the presence of meridional gradients of surface temperature. While the presumably low efficiency of the atmospheric engine has been blamed on the hydrological cycle (e.g., Pauluis, 2011), our analysis suggests a different source of inefficiencies.

In the upper atmosphere the discrepancy between the theoretical and observed pressure distributions is apparently more significant (Fig. 8): over this larger range in altitude the lapse rate variation finally plays in. However, to justify our main conclusion – highlighting cancellation of kinetic energy among cells through processes primarily related to surface temperature – it is sufficient to capture the horizontal pressure difference at the height h_m where kinetic energy generation is maximum.

For the Hadley cells, the theoretical and observed pressure difference remain close from $z = 0$ up to $z \approx h_m$. For $z > h_m$ the observed pressure difference declines more rapidly than does the theoretical one. For this reason, while the estimated top of the troposphere h_T is located higher than h_m , the theoretical pressure difference estimated by us for $z = h_T$ (Table 2) is very similar to the observed pressure difference at h_m (Fig. 8). In the Ferrel cells h_T and h_m approximately coincide, while the discrepancy between the theoretical and observed pressure distribution is larger than in the Hadley cells but never exceeds 30%. Overall, Fig. 8 makes it clear that Eqs. (27) and (28), which focus on surface temperature and pressure differences, satisfactorily capture the behavior of the pressure difference across the circulation cells and thus provide a reasonable first-order estimate for the relationship between work outputs of the Earth’s major heat engines and heat pumps.

Appendix C. Spatial variation of lapse rate in the lower atmosphere

Here we show that Eq. (25) remains valid in the presence of spatial variation in temperature lapse rate $\Gamma \equiv -\partial T/\partial z$ if under ΔT_s in Eq. (25) we understand the horizontal temperature difference at one half the mean height of the lower streamline. In the formulae below $T \equiv T(y, z) = T_s(y) - \Gamma(y)z(y)$, $p \equiv p(y, z) = p_s(y)[T(y, z)/T_s(y)]^{1/c(y)}$, where $T_s(y)$ is surface temperature and $p_s(y)$ is surface pressure.

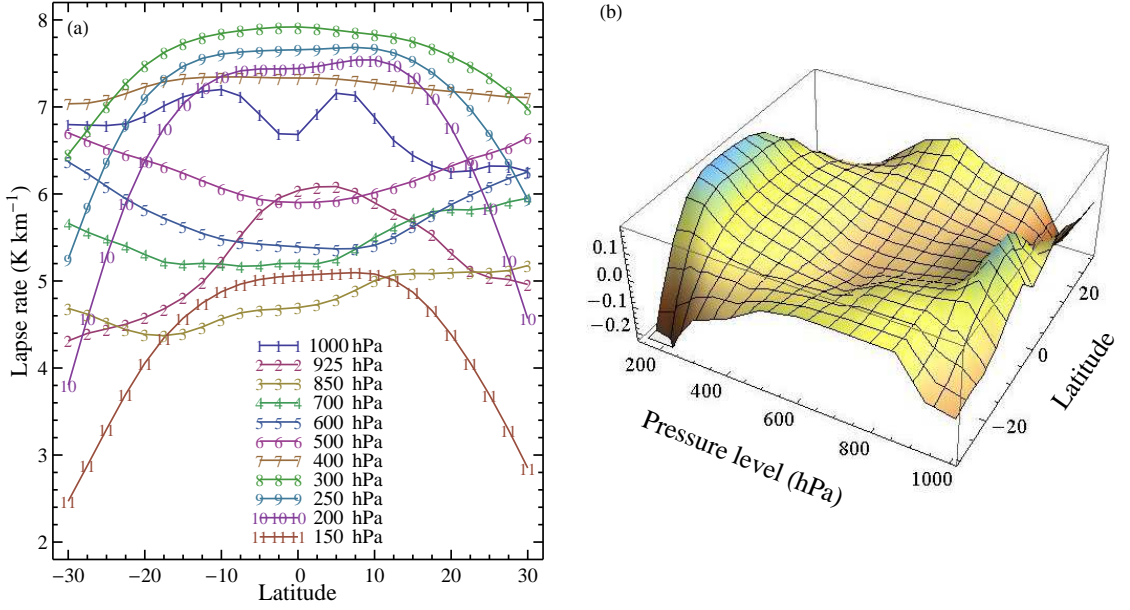


Figure 9: Annual mean latitudinal profiles of the air temperature lapse rate on different pressure levels. For example, curve 1 in (a) shows the mean lapse rate between 1000 hPa and 925 hPa; curve 2 – between 925 hPa and 850 hPa; curve 11 – between 150 and 100 hPa. Panel (b) shows the relative horizontal variation – at each pressure level the lapse rate at a given latitude is divided by the mean lapse rate at this level (averaged between 30°S and 30°N). The equator has a higher lapse rate than the 30th latitudes in the lower and upper – but not the middle – troposphere. The data are long-term mean NCEP-NCAR climatology (see Section 6).

Using these relationships we find

$$\frac{RT}{p} \frac{\partial p}{\partial y} \Big|_{z=z(y)} = \frac{RT}{p_s} \frac{\partial p_s}{\partial y} + \Psi, \quad (33)$$

$$\Psi \equiv \frac{RT}{c} \left(\frac{1}{T} \frac{\partial T}{\partial y} - \frac{1}{T_s} \frac{\partial T_s}{\partial y} - \frac{1}{c} \frac{\partial c}{\partial y} \ln \frac{T}{T_s} \right).$$

Expanding the logarithm in Eq. (33) over $\Gamma z/T_s \ll 1$

$$\ln \frac{T}{T_s} = \ln \left(1 - \frac{\Gamma z}{T_s} \right) = -\frac{\Gamma z}{T_s} - \frac{1}{2} \left(\frac{\Gamma z}{T_s} \right)^2, \quad (34)$$

we find from Eq. (34) (note that $R/c = Mg/\Gamma$ and $T/T_s = 1 - \Gamma z/T_s$)

$$\Psi = Mgz \left(\frac{1}{T_s} \frac{\partial T_s}{\partial y} - \frac{z}{2T_s} \frac{\partial \Gamma}{\partial y} - \frac{1}{z} \frac{\partial z}{\partial y} \right). \quad (35)$$

When Ψ is integrated over the boundary layer of a fixed height, i.e. when $z(y_1) = z(y_2)$, the last term in Eq. (35) vanishes.

Noting that $\Gamma z \ll T$, $T \approx T_s$ and $\Delta p_s \ll p_s$ and that we defined $\Delta p_s \equiv - \int_{y_1}^{y_2} (\partial p_s / \partial y) dy$,

the kinetic energy generation in the presence of lapse rate variation A_Γ becomes, cf. Eq. (25):

$$A_\Gamma \equiv - \int_{y_1}^{y_2} \frac{RT}{p} \frac{\partial p}{\partial y} \Big|_{z=z(y)} dy$$

$$\approx Mgh_s \left[\frac{\Delta p_s}{p_s} - \frac{\bar{z}}{h_s} \frac{\Delta T}{T_s} \right], \quad (36)$$

$$\Delta T \equiv \Delta T_s - \Delta \Gamma \frac{\bar{z}}{2}. \quad (37)$$

Here ΔT is the horizontal temperature difference at a height equal to one half of the mean streamline height \bar{z} .

Equation (36) allows us to conclude that with a small $\bar{z} \sim 1$ km any horizontal variation in lapse rate makes a minor contribution to kinetic energy generation. (The vertical variation in Γ is zero in the first approximation, again because z is small). For example, even if in the boundary layer the lapse rate changes by $\Delta \Gamma = 4$ K km⁻¹ (which is approximately the difference between the dry and moist adiabatic lapse rates), the lapse rate term in Eq. (36) will be negligible compared to the pressure term: $(\bar{z}/h_s)(\Delta \Gamma \bar{z})/(2T_s) \sim 0.7 \times 10^{-4} \ll \Delta p_s/p_s \sim 10^{-2}$.

Note that in the real atmosphere the horizontal variation in lapse rate is smaller. For example, the zonally averaged lapse rate between 925 and 850 hPa changes across the Hadley cells by about 2 K km⁻¹ (Fig. 9). Notably, in the lower atmosphere the equatorial areas of the Hadley cells have a larger lapse rate than the higher latitudes ($\Delta \Gamma > 0$). This lapse rate variation makes a positive contribution to the kinetic energy generation similar to the positive contribution of the negative surface temperature gradient in the Ferrel cells.

In severe hurricanes the horizontal variation in lapse rate across the hurricane area can be about $\Delta \Gamma = -4$ K km⁻¹ (e.g., Montgomery et al., 2006, their Fig. 4c) in the lower 2 km. This variation makes a negative contribution to kinetic energy generation. But in these circulation systems $\Delta p_s/p_s > 5 \times 10^{-2}$ is several times greater than in the zonally averaged cells, so the pressure term in Eq. (36) remains the main one. These considerations indicate that in the lower atmosphere kinetic energy generation is determined by surface pressure gradients.

References

- Bates, J. R. 2012. Climate stability and sensitivity in some simple conceptual models. *Climate Dynamics* **38**, 455–473.
- Bayr, T. and Dommenges, D. 2013. The tropospheric land-sea warming contrast as the driver of tropical sea level pressure changes. *J. Climate* **26**, 1387–1402.
- Bony, S., Stevens, B., Frierson, D. M. W., Jakob, C., Kageyama, M., Pincus, R., Shepherd, T. G., Sherwood, S. C., Siebesma, A. P., Sobel, A. H., Watanabe, M., and Webb, M. J. 2015. Clouds, circulation and climate sensitivity. *Nature Geoscience* **8**, 261–268.
- Boville, B. A. and Bretherton, C. S. 2003. Heating and kinetic energy dissipation in the NCAR Community Atmosphere Model. *J. Climate* **16**, 3877–3887.
- Cai, M. and Shin, C.-S. 2014. A total flow perspective of atmospheric mass and angular momentum circulations: boreal winter mean state. *J. Atmos. Sci.* **71** 2244–2263.
- Chen, G., Held, I. M., and Robinson, W. A. 2007. Sensitivity of the latitude of the surface westerlies to surface friction. *J. Atmos. Sci.* **64**, 2899–2915.
- Dobrovolski, R. and Rattis, L. 2015. Water collapse in Brazil: the danger of relying on what you neglect. *Natureza & Conservação* **13**, 80–83.

- Heffernan, O. 2016. The mystery of the expanding tropics. *Nature* **530**, 20–22.
- Held, I. M. and Hou, A. Y. 1980. Nonlinear axially symmetric circulations in a nearly inviscid atmosphere. *J. Atmos. Sci.* **37**, 515–533.
- Huang, J. and McElroy, M. B. 2014. Contributions of the Hadley and Ferrel circulations to the energetics of the atmosphere over the past 32 years. *J. Climate* **27**, 2656–2666.
- Huang, J. and McElroy, M. B. 2015. A 32-year perspective on the origin of wind energy in a warming climate. *Renewable Energy* **77**, 482–492.
- Johnson, D. R. 1989. The forcing and maintenance of global monsoonal circulations: An isentropic analysis. *Advances in Geophysics* **31**, 43–316.
- Kalnay, E., Kanamitsu, M., Kistler, R., Collins, W., Deaven, D., Gandin, L., Iredell, M., Saha, S., White, G., Woollen, J., Zhu, Y., Leetmaa, A., Reynolds, B., Chelliah, M., Ebisuzaki, W., Higgins, W., Janowiak, J., Mo, K. C., Ropelewski, C., Wang, J., Jenne, R., and Joseph, D. 1996. The NCEP/NCAR 40-year reanalysis project. *Bull. Amer. Meteor. Soc.* **77**, 437–471.
- Kieu, C. 2015. Revisiting dissipative heating in tropical cyclone maximum potential intensity. *Quart. J. Roy. Meteorol. Soc.* **141**, 2497–2504.
- Kim, Y.-H. and Kim, M.-K. 2013. Examination of the global Lorenz energy cycle using MERRA and NCEP-reanalysis 2. *Climate Dynamics* **40**, 1499–1513.
- Lindzen, R. S. and Nigam, S. 1987. On the role of sea surface temperature gradients in forcing low-level winds and convergence in the tropics. *J. Atmos. Sci.* **44**, 2418–2436.
- Lorenz, R. D. and Rennó, N. O. 2002. Work output of planetary atmospheric engines: dissipation in clouds and rain. *Geophys. Res. Lett.* **29**, 10–1–10–4.
- Makarieva, A. M., Gorshkov, V. G., Li, B.-L., and Nobre, A. D. 2010. A critique of some modern applications of the Carnot heat engine concept: the dissipative heat engine cannot exist. *Proc. R. Soc. A* **466**, 1893–1902.
- Makarieva, A. M., Gorshkov, V. G., and Nefiodov, A. V. 2014. Condensational power of air circulation in the presence of a horizontal temperature gradient. *Phys. Lett. A* **378**, 294–298.
- Makarieva, A. M., Gorshkov, V. G., and Nefiodov, A. V. 2015a. Empirical evidence for the condensational theory of hurricanes. *Phys. Lett. A* **379**, 2396–2398.
- Makarieva, A. M., Gorshkov, V. G., Nefiodov, A. V., Sheil, D., Nobre, A., and Li, B.-L. 2015b. Reassessing thermodynamic and dynamic constraints on global wind power. <http://arxiv.org/abs/1505.04543>.
- Makarieva, A. M., Gorshkov, V. G., Nefiodov, A. V., Sheil, D., Nobre, A. D., Bunyard, P., and Li, B.-L. 2013a. The key physical parameters governing frictional dissipation in a precipitating atmosphere. *J. Atmos. Sci.* **70**, 2916–2929.
- Makarieva, A. M., Gorshkov, V. G., Nefiodov, A. V., Sheil, D., Nobre, A. D., and Li, B.-L. 2015c. Comments on "The tropospheric land-sea warming contrast as the driver of tropical sea level pressure changes". *J. Climate* **28**, 4293–4307.
- Makarieva, A. M., Gorshkov, V. G., Sheil, D., Nobre, A. D., and Li, B.-L. 2013b. Where do winds come from? A new theory on how water vapor condensation influences atmospheric pressure and dynamics. *Atmos. Chem. Phys.* **13**, 1039–1056.

- Marengo, J. A. and Espinoza, J. C. 2016. Extreme seasonal droughts and floods in Amazonia: causes, trends and impacts. *Int. J. Climatol.* **36**, 1033–1050.
- Marvel, K., Kravitz, B., and Caldeira, K. 2013. Geophysical limits to global wind power. *Nature Climate Change* **3**, 118–121.
- Montgomery, M. T., Bell, M. M., Aberson, S. D., and Black, M. L. 2006. Hurricane Isabel (2003): New insights into the physics of intense storms. Part I: Mean vortex structure and maximum intensity estimates. *Bull. Amer. Meteor. Soc.* **87**, 1335–1347.
- Pauluis, O. 2011. Water vapor and mechanical work: A comparison of Carnot and steam cycles. *J. Atmos. Sci.* **68**, 91–102.
- Pauluis, O., Balaji, V., and Held, I. M. 2000. Frictional dissipation in a precipitating atmosphere. *J. Atmos. Sci.* **57**, 989–994.
- Peixoto, J. P. and Oort, A. H. 1992. *Physics of Climate*. American Institute of Physics, New York.
- Pielke, R. A. 1981. An overview of our current understanding of the physical interactions between the sea- and land-breeze and the coastal waters. *Ocean Manage.* **6**, 87–100.
- Rienecker, M. M., Suarez, M. J., Gelaro, R., Todling, R., Bacmeister, J., Liu, E., Bosilovich, M. G., Schubert, S. D., Takacs, L., Kim, G.-K., Bloom, S., Chen, J., Collins, D., Conaty, A., da Silva, A., Gu, W., Joiner, J., Koster, R. D., Lucchesi, R., Molod, A., Owens, T., Pawson, S., Pegion, P., Redder, C. R., Reichle, R., Robertson, F. R., Ruddick, A. G., Sienkiewicz, M., and Woollen, J. 2011. MERRA: NASA’s modern-era retrospective analysis for research and applications. *J. Climate* **24**, 3624–3648.
- Robinson, W. A. 1997. Dissipation dependence of the jet latitude. *J. Climate* **10**, 176–182.
- Santer, B. D., Sausen, R., Wigley, T. M. L., Boyle, J. S., AchutaRao, K., Doutriaux, C., Hansen, J. E., Meehl, G. A., Roeckner, E., Ruedy, R., Schmidt, G., and Taylor, K. E. 2003. Behavior of tropopause height and atmospheric temperature in models, reanalyses, and observations: Decadal changes. *J. Geophysical Research: Atmospheres* **108**, ACL 1–1–ACL 1–22.
- Schneider, T. 2006. The general circulation of the atmosphere. *Annu. Rev. Earth Planet. Sci.* **34**, 655–688.
- Shepherd, T. G. 2014. Atmospheric circulation as a source of uncertainty in climate change projections. *Nature Geoscience* **7**, 703–708.
- Webster, P. J. 2004. The Elementary Hadley Circulation. In Diaz, H. F. and Bradley, R. S., editors, *The Hadley Circulation: Past, Present and Future*, volume 21 of *Advances in Global Change Research*, pages 9–60. Kluwer Academic Publishers.
- Wulf, O. R. and Davis Jr., L. 1952. On the efficiency of the engine driving the atmospheric circulation. *J. Meteorol.* **9**, 79–82.